J. Min. Metall. Sect. B-Metall. 60 (1) (2024) 139 - 152

Journal of Mining and Metallurgy, Section B: Metallurgy

EFFECTS OF CeO_2/Y_2O_3 RARE EARTH OXIDES ON THE MICROSTRUCTURE AND PROPERTIES OF AN IN-SITU SYNTHESIZED WC-REINFORCED NI-BASED CLADDING LAYER

C.-X. Zhang, W.-C. Sun*, E.-Y. Liu, Y.-W. Liu, J.-P. Liu, B. Zhang, Y.-F. Xu, M.-R. Zhou**

College of Materials Science and Engineering, Xi'an University of Science and Technology, Xi'an, Shaanxi, China

(Received 13 October 2023; Accepted 04 June 2024)

Abstract

A novel tungsten carbide (WC)-reinforced nickel (Ni)-based laser cladding layer was prepared through an in-situ synthesis process. The influence of different concentrations of CeO_2/Y_2O_3 on the microstructure, wear, and corrosion resistance of the in-situ synthesized WC-reinforced Ni-based cladding layer was analyzed. The results revealed that the coatings doped with rare-earth oxides exhibited good micro-hardness (660 HV0.2) and wear resistance when the rare-earth oxide content reached 0.75% CeO_2 and 1.50% Y_2O_3. Additionally, the minimum corrosion rates of the coating were measured at 0.002770 mm/a and 0.0022548 mm/a at 1.5% CeO_2 and 1.5 Y_2O_3 doping, with noble E_{corr} values ranging from -0.12549 V to -0.49924 V and lower I_{corr} values ranging from 2.3550×10^{-7} A·cm^2 to 1.9170×10^{-7} A·cm^2. Furthermore, the wear resistance of the cladding layer was significantly higher than that of the substrate. Both the cladding layer and the substrate exhibited a mixed-wear mode, and they exhibit adhesive wear in wet friction environments.

Keywords: *Laser cladding; In-situ synthesized; Rare earths; Mechanical properties; Electrochemical properties*

1. Introduction

Wear and corrosion resistance are the main challenges in the application of mining hydraulic support ball valves and coal mine interceptors, which operate in harsh environments [1,2]. Therefore, in order to improve the overall performance of the alloy material, formation/deposition of a coating on the surface of the material is an effective and economical method [3,4]. Composite coatings that contain two or more metallic elements typically exhibit excellent mechanical and chemical properties, which is due to the favorable correspondence between their crystal lattices [5-7].

The doping of ceramic particles with hard phases can effectively enhance the performance of laser cladding layers. However, direct doping of particles of different particle size or density from the fused powder to enhance the properties of the cladding layer is prone to the generation of pores and cracks due to the irregular microstructure of the powder particles and the substrate, particle aggregation, and powder surface contamination [8]. In contrast, in-situ synthesized reinforced phase overcomes these problems because the reinforcement is uniformly distributed in the coating, which has good interfacial compatibility, so that various properties of the cladding layer, such as micro-hardness and wear resistance, are upgraded [9,10].

Despite the various excellent properties of laser cladding coatings, inherent defects such as cracks, porosity and inclusions cannot be avoided [11-13]. Previous studies have shown that adding appropriate amounts of rare earth oxides can effectively avoid these defects [14-16]. Rare earth elements are active elements, mainly due to the exchange of electrons and the polarization between atoms, which can easily change the size of atoms [17-19]. Therefore, rare earth elements easily react with other elements during the cladding process and form stable compounds [20]. The addition of small amounts of rare earth elements to the laser cladding layer could significantly improve the tribomechanical properties [21], such as surface micro-hardness, elastic modulus, fracture toughness, and friction coefficient. In addition, rare earth elements in the coating material system improve wetting properties [22], increase coating toughness [23], reduce cracking tendency [24], and improve corrosion resistance [25].

In this work, the in-situ synthesized WC-reinforced nickel-based laser cladding layer was prepared. The effect of doping CeO_2/Y_2O_3 rare earth oxides with different mass percentages on the microstructure and properties of the in-situ

*Corresponding author: *sunwanchang@tsinghua.org.cn; **liueryong@xust.edu.cn*

https://doi.org/10.2298/JMMB231013012Z

synthesized WC-reinforced nickel-based cladding layer was investigated.

2. Materials and methods

2.1. Materials

2.1.1. Substrate material

The normalized 45# steel plate is selected as the base material for this test due to its improved cutting properties and higher comprehensive mechanical properties, including strength and toughness. To begin, the plate is wire cut into dimensions of 150 mm×90 mm×20 mm. Subsequently, the surface of the substrate is meticulously sanded using 400#, 800#, and 1000# sandpaper to achieve a smooth finish. Furthermore, the surface of the substrate is cleaned with anhydrous ethanol and blown dry for use.

2.1.2. Melting powder

The powders used for the cladding layer are Ni60 powder, WO_3 powder, B_4C powder, pure Al powder, CeO_2 powder and Y_2O_3 powder. The quantity of doped (WO_3+B_4C+Al) mixed powder was 25%. The relevant parameters of the powder and the chemical composition and content of Ni60 powder are given in Table 1.

Table 1. *The relevant parameters of the powder and the chemical composition and content of Ni60 powder*

(a) Cladding powder						
Power	Particle size	Purity	Manufacturer			
Ni60	50-100μm	99.90%	Kennametal Stellite Co.,Ltd			
WO_3	25μm	99.90%	CMT Xindun Alloy Welding Spraying Co.,Ltd			
B_4C	5μm	99.90%	Mudanjiang Jingangzuan Boron Carbide Co.,Ltd			
Al	75μm	99.90%	Shanghai Hasu Industry & Trade Co.,Ltd			
CeO_2	1 μm	99.90%	Shanghai Meiyi Alloy Materials Co.,Ltd			
Y_2O_3	1 μm	99.90%	Shanghai Meiyi Alloy Materials Co.,Ltd			
(b) The chemical composition and content of Ni60 powder (wt.%)						
C	Cr	Si	W	B	Fe	Ni
0.8	15.5	4	3	3.5	15	Bal.

2.2. Cladding layer preparation

The pre-configured molten powder was placed in a beaker according to a percentage of mass, a certain amount of anhydrous ethanol was added, and the powder was mechanically stirred for 4.5 h.

After that, the powder was put into a vacuum drying oven and dried at 90 °C for 8 h. Finally, the powder was sealed and stored for use.

In this experiment, the in-situ synthesized WC ceramic particles reinforced with Ni-based laser cladding layer were prepared by the pre-positioning method. Using anhydrous ethanol as the binder, the dried powder was mixed into a paste, and then it was uniformly pre-coated onto the surface of 45# steel plate with a coating thickness of 1.5-2 mm and a pre-coating width of 1.5 mm. The 45# steel plate with the pre-placed metal powder was preheated in a vacuum drying oven at 200 °C for 4 h. Subsequently, it was removed, and the laser cladding equipment was used for cladding layer preparation. The laser power was 3000 W, the scanning rate was 3 mm/s.

Three depositions of powders with different contents were performed, from which a cut sample was selected for characterization.

2.3. Characterization of the cladding layer

The surface and cross-sectional morphologies of cladding layer were viewed by using a scanning electron microscope (SEM) (JSM-6390A, JEOL, Japan) with a voltage of 20 kV and a gun/cathode type of tungsten filament.

The crystal phase of the cladding layer was analyzed by X-ray diffraction (XRD; X'Pert PRO MPD, Malvern Panalytical, Netherlands).

The micro-indentation hardness of the cladding layer surface was measured by using a micro-Vickers hardness tester (EM-1500L, Shanghai Everone Ltd, China) under a load of 200 gram-force for 10 s. The final micro-indentation hardness is the statistical average of ten measurements conducted at different points with a space of 40 μm.

The anti-wear features of the cladding layer were evaluated by using a friction and wear tester (MFT-R4000, Lanzhou Huahui Instrument Technology Co., Ltd, China) at ambient temperature, and a silicon carbide ball with a diameter of 3.5 mm was run on the sample with a load of 25 N for 60 min.

3. Results and discussion

3.1. Effect of Rare Earth Doped on Microstructure of Cladding Layer

3.1.1. Phase composition

Figure 1(a) shows the XRD patterns of the in situ grown WC-reinforced nickel-based melt cladding layer doped with different contents of CeO_2, from which the main phases of the CeO_2-doped melt cladding layer are γ-(NiFe) solid solution, $Cr_{23}C_6$ phase, Al_2O_3, W_2C, WC, CeO_2, $CeNi_5$ and WB_2 phases, and weak WC_3, WB_4, $Ce_3Ni_6Si_2$ and WC_{1-x} phase diffraction peaks. With the gradual increase of the doped CeO_2 content. The peak is strongest at a CeO_2 doping level of 1.25%, indicating that the relative content of in-situ synthesized WC grains is the highest. In addition, the peak of 1% CeO_2 doping is shifted to the right indicating a change in the lattice parameters. It may be due to the doping of $CeNi_5$, which is smaller than the main body Ni60, making the cell parameters smaller, and the spacing between the crystal surfaces is smaller, causing the peak position shift. Meanwhile, the XRD pattern shows that the rare-earth oxide CeO_2 chemically reacted with Ni60 powder during the melt coating process to generate stable rare-earth compounds $CeNi_5$ and $Ce_3Ni_6Si_2$, which have good strengthening effect on the properties of the melt coating layer.

Figure 1(b) shows the XRD patterns of the in situ grown WC-reinforced nickel-based melt cladding layer doped with different contents of Y_2O_3. The main phases of the melt cladding layer are basically unchanged, except for the rare earth compound phase. The main phases are the γ-(NiFe) solid solution, the $Cr_{23}C_6$ phase, the Al_2O_3, W_2C, WC, Y_2O_3, $Ni_{17}Y_3$, YAl_3 and WB_2 phases, and the weak WC_3, WB_4, AlNiY and WC_{1-x} phase diffraction peaks. The intensity of the diffraction peaks of the Y_2O_3-doped fused cladding layer is raised compared to that of the undoped layer. The Y_2O_3-doped cladding layer undergoes a chemical reaction during solidification to produce stable rare-earth compounds $Ni_{17}Y_3$, YAl_3 and AlNiY phases, which have a positive effect on the improvement of the cladding layer properties.

3.1.2. Microstructures

Figures 2 and 4 show the morphologies of typical in-situ synthesized WC particles in the coatings, where the shape of the WC particles is mainly a combination of triangles and quadrilaterals. No holes or cracks were found in the in-situ synthesized coating and the WC reinforcing phase was uniformly distributed throughout the coating. This result highlights the effectiveness of the in-situ synthesis method in enhancing the interfacial affinity and cohesion between the reinforcing phase and the parent material. This is due to the fact that in-situ synthesized WC particles are clean from Ni substrates [26]. This results in in-situ synthesized composite coatings with high tungsten carbide content and high density. The mechanical properties of the coatings can be greatly enhanced.

Figure 2 shows the full cross-sectional view and the top/middle/bottom region of the in-situ synthesized WC-reinforced nickel-based cladding layer doped with different contents of CeO_2. As the CeO_2 content increases from 0 to 1%, some of the enhanced-phase particles in the CeO_2-doped cladding gradually decrease, but more particles are promoted to aggregate and coarsen into larger particles. With the increase of CeO_2 content, the dissolution and decarburization of WC hard phase particles in the cladding layer became more and more serious, and some lamellar secondary precipitation phases were formed around the hard phase particles in the cladding layer, and some plane and cellular crystals were formed at the bottom of the cladding layer. Figures 2

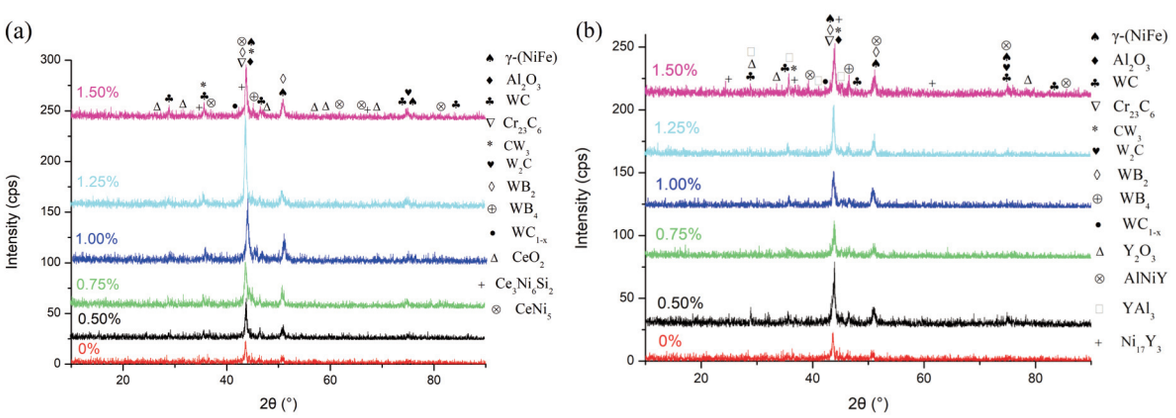

Figure 1. *XRD pattern of in-situ synthesized WC reinforced nickel base cladding layer: (a) different content of CeO_2, (b) different content of Y_2O_3*

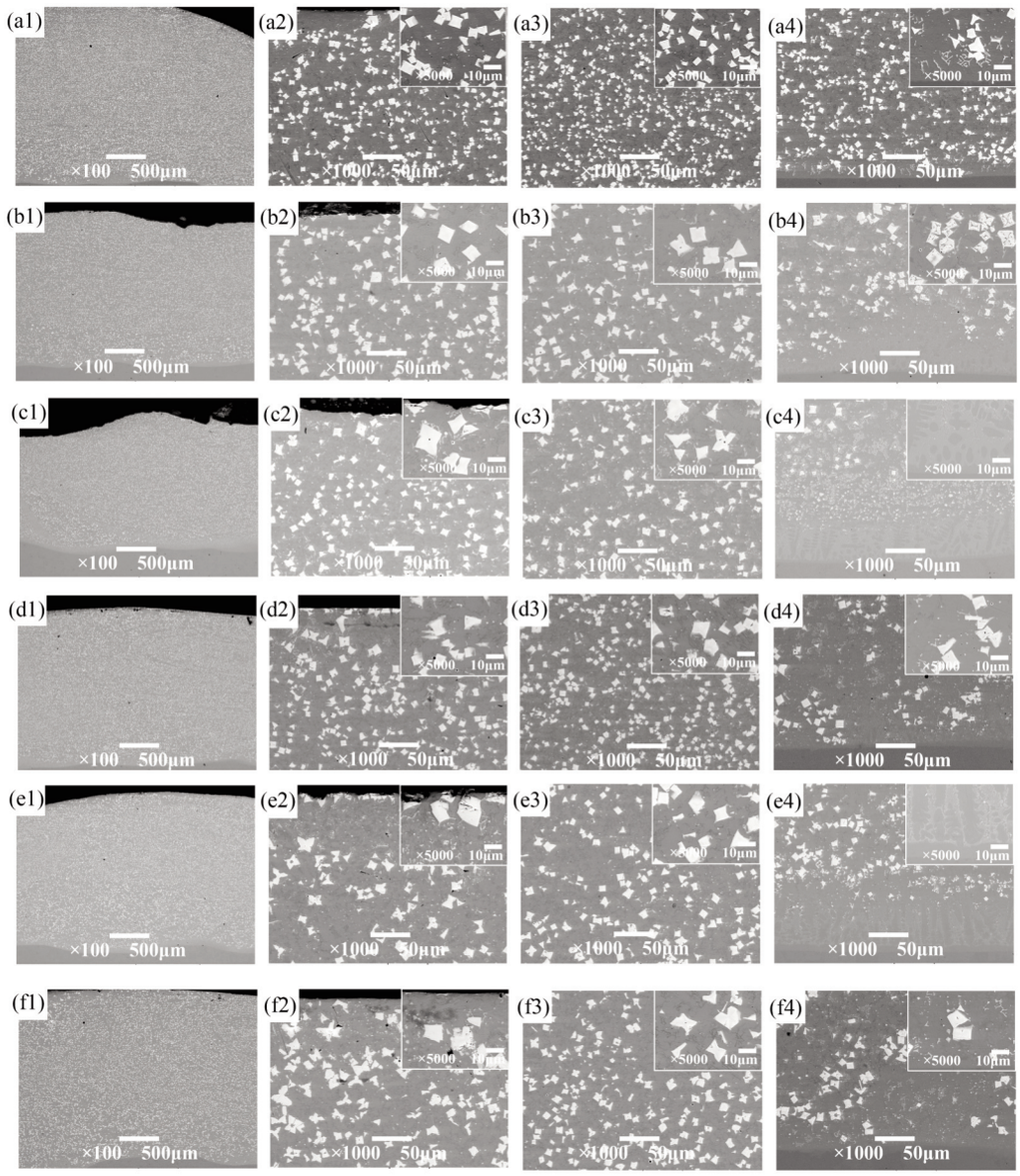

Figure 2. *The microstructure morphologies of in-situ synthesized WC reinforced nickel base cladding layer with different content of CeO_2: (a) 0%, (b) 0.50%, (c) 0.75%, (d) 1.00%, (e) 1.25%, (f) 1.50%; (1) cross-sectional panorama, (2) morphologies of the upper region, (3) morphologies of the middle region, (4) morphologies of the lower region*

(b4-f4) indicate that the in-situ reaction primarily occurs in the middle and upper sections of the coating, which could be attributed to the upward movement of doped Al powder and B_4C powder during the melting process, leading to the reaction in the middle and upper regions of the cladding. As a result, the lower part of the cladding either lacks or contains a small amount of smaller WC clumps.

When the content of CeO_2 was 1.00%, the WC hard-phase particles in the cladding were significantly reduced and more uniform in size and distribution. However, when the content of CeO_2 was 1.25%, the WC hard phase particles in the cladding layer showed an obvious aggregation phenomenon, the particles appeared to increase, the particle distribution was less uniform compared with other cladding layers, and the area of forming plane and cellular crystals at the bottom of the cladding layer was wider. When the content of CeO_2 was 1.50%, the WC hard phase particles at the bottom of the cladding layer appeared a small amount of flaky secondary precipitation phase. This may be that the cladding layer was subject to a more intense aluminothermic reaction, releasing the heat which promoted the dissolution and

reprecipitation of the WC phases and the formation of the lamellar W-rich eutectic structures [27].

As can be seen in Figure 2(b4-f4), the WC-reinforced phase particles at the bottom of the CeO_2-doped cladding layer are smaller than those in the upper region, which is due to the solidification characteristics of the melt pool during the laser cladding process. The bottom of the cladding layer dissipates heat faster and solidifies at a faster rate, so the nucleation time of the WC particles of the enhancement phase is shorter, resulting in smaller WC ceramic phase particles. Generally speaking, the more WC-reinforced phase particles in the cladding layer, the higher the micro-hardness of the cladding layer will be. However, the effect of WC-reinforced phase content is only one aspect, the morphological characteristics and the size of the particles also have a greater influence on the micro-hardness of the cladding layer.

Figure 3 shows the morphology of the WC hard particle-enhanced phase skeleton formed after corrosion of the in situ grown WC-reinforced nickel-based molten cladding layer doped with 1.00% CeO_2. The morphology of WC crystals was initially nucleated in a nearly spherical morphology, and then grew continuously, and the mirrors with small surface energy gradually disappeared during the growth process, so that the WC particles gradually grew into polyhedral up to hexagonal prisms, and finally grew into trigonal crystal morphology under the further action of interfacial energy [28], which is consistent with the morphology of the cladding layer after corrosion in Fig. 3, which shows the same hard phase particle morphology. In Fig. 3, the multi-prismatic crystals are WC reinforced phase particles, while the other fine columnar particles are intermetallic compounds and the rare earth oxides are distributed at the grain boundaries. And the rarer earth compounds were formed at the grain boundaries as the addition of rare earth elements continued to increase [29,30].

Figure 4 shows the full view and the top/middle/bottom region tissue morphology of the in-situ synthesized WC-reinforced nickel-based melt cladding layer doped with different contents of Y_2O_3, from which it can be seen that the morphology in the melt cladding layer does not reveal deeper holes and longitudinal penetration cracks, mainly because the addition of rare earth oxides improved the fluidity of the melt pool and facilitated the gas discharge from the melt pool, thus eliminating the pores and cracks in the cladding layer [29,30]. With the addition of Y_2O_3, the stress concentration generated between the matrix and the reinforcing phase was greatly reduced, and the rare earth compounds can easily aggregate to the grain boundaries through nucleation and growth rejection due to the large radius of rare earth element yttrium. A large amount of rare earth element yttrium deflects, pins and adsorbs at the active sites of grain boundaries during crystal growth, which reduced the Gibbs free energy of the system and the driving force of grain growth, inhibit the diffusion of nickel, aluminum and chromium atoms, thus hindering the crystal growth and intensifying its branching, and also promoting the appearance of more and more lamellar secondary precipitation phases in the molten cladding layer with the increasing Y_2O_3 content. In addition, with the increase of doped Y_2O_3 content, some small WC phase particles gradually appeared in the molten cladding layer to gather and grow into larger particles, and agglomeration phenomenon appears.

The particle size and distribution of WC hard particles in the cladding layer were more uniform when the Y_2O_3 content was 1.25%, indicating that the Y_2O_3 doping was optimal. Compared with the undoped Y_2O_3 cladding layer in Fig. 4(a), the content of Y_2O_3 doped has less of effect on the in-situ synthesized of WC hard particles. The cladding layer without Y_2O_3 doped had smaller WC hard particles and more uniform distribution.

When the Y_2O_3 content was 1.25%, the particle size and distribution of WC hard particles in the cladding layer were more uniform, and the Y_2O_3 doping amount was optimal at this time, but compared with the cladding layer without Y_2O_3 doping in Fig. 4(a), the Y_2O_3 doping had less positive effect on the in-situ growth of WC hard particles in this scheme to enhanced the nickel-based cladding layer from the microstructure morphology, and the cladding layer without Y_2O_3 doping had smaller WC hard particles and more uniform distribution. The WC hard particles

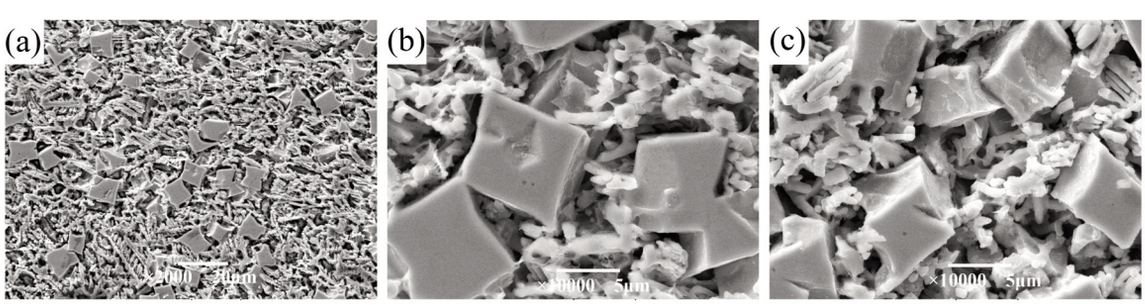

Figure 3. *The morphologies of WC hard particle reinforced phase skeleton formed after corrosion of in-situ synthesized WC reinforced nickel base cladding layer doped with 1.00% CeO_2: (a) ×2000, (b) ×10000, (c) ×10000*

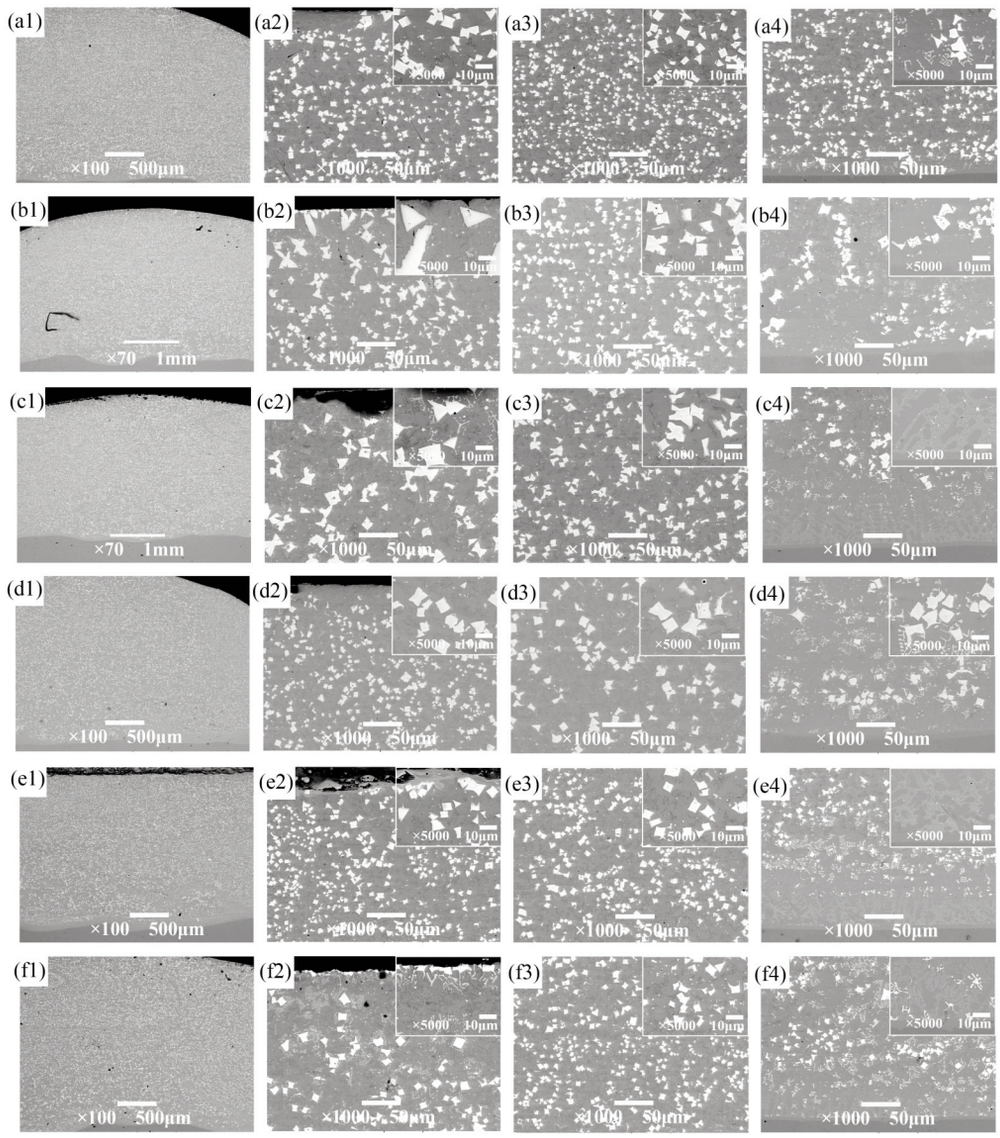

Figure 4. *The microstructure morphologies of in-situ synthesized WC reinforced nickel base cladding layer with different content of Y2O3: (a) 0%, (b) 0.50%, (c) 0.75%, (d) 1.00%, (e) 1.25%, (f) 1.50%; (1) cross-sectional panorama, (2) morphologies of the upper region, (3) morphologies of the middle region, (4) morphologies of the lower region*

in the undoped Y_2O_3 layer were smaller and more uniformly distributed. When the Y_2O_3 content was 1.5%, the in-situ synthesized WC particles in the top area of the cladding layer appear to be aggregated, and multiple blocks appear to be connected, and more lamellar secondary precipitation phases were distributed around the block particles, and there were fewer WC particles at the bottom of the cladding layer, and the WC particles basically dissolved and decarburized, forming a large number of secondary precipitation phases uniformly distributed at the bottom of the cladding layer. At the same time, the bottom of the cladding layer showed a narrower plane crystal region and a wider cellular crystal region.

3.2. Effect of rare earth doped on the micro-hardness and frictional wear properties of the cladding layer

3.2.1. Micro-hardness

The surface micro-hardness histograms and cross-sectional micro-hardness profiles of the in situ grown WC-reinforced nickel-based cladding layers doped with different CeO_2 contents are shown in Figure 5, respectively. The results indicate that the cladding layer doped with the rare earth oxide CeO_2 has a

slightly lower micro-hardness compared to the undoped cladding layer. This is likely due to the refining effect of CeO_2 on the grains during the cladding process, resulting in smaller WC hard phase particles in the cladding layer [27]. The micro-hardness of the cladding layers exceeds that of the 45# steel matrix, indicating the presence of a significant amount of in-situ synthesized WC hard reinforced phase in the cladding layers.

Figure 5(b) shows that the micro-hardness value increases slightly with the gradual increase of CeO_2 content. The molten cladding layer exhibits less fluctuation of micro-hardness value in the cross section, and there is a transition zone of micro-hardness value between the matrix and the molten cladding layer, which is roughly distributed on both sides of the molten cladding layer interface, indicating that there is a good transition zone of composition between the molten cladding layer and the matrix. When doped with 1.00% CeO_2, the micro-hardness of the cladding layer reached a maximum value of approximately 860 HV0.2, which was approximately 3.3 times the value of the matrix micro-hardness (about 260 HV0.2).

Figure 6 shows the histograms of the surface micro-hardness and the curves of cross-sectional micro-hardness distribution of the nickel-based cladding layers reinforced with in-situ synthesized WC and doped with varying Y_2O_3 contents. The surface micro-hardness of the cladding layer doped with varying Y_2O_3 content is slightly lower than that of the undoped cladding layer. This also indicates that Y_2O_3 has a better refining effect on the hard particles in the cladding layer during the in-situ growth process. With the gradual increase of Y_2O_3 content, the micro-hardness of the cladding layer slightly decreased, but the micro-hardness values of all cladding layers were between 3-5 times of the micro-hardness of the base material, indicating that the micro-hardness value of the cladding layer became smaller when the WC particles were smaller. The micro-hardness value of the cladding layer reached its maximum value of about 870 HV0.2 when the Y_2O_3 content was 0.75%.

Fig. 6(b) shows that the micro-hardness values on each cladding layer are evenly distributed, showing a more uniform hard phase distribution. However, when the Y_2O_3 content was 0.75%, the micro-hardness

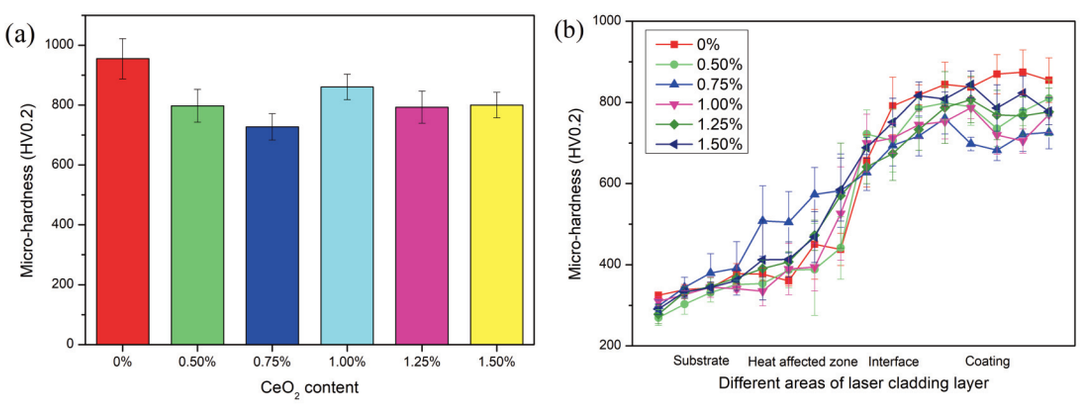

Figure 5. *The micro-micro-hardness of in-situ synthesized WC reinforced nickel base cladding layer with different content of CeO_2: (a) the surface micro-micro-hardness, (b) the cross-section micro-micro-hardness*

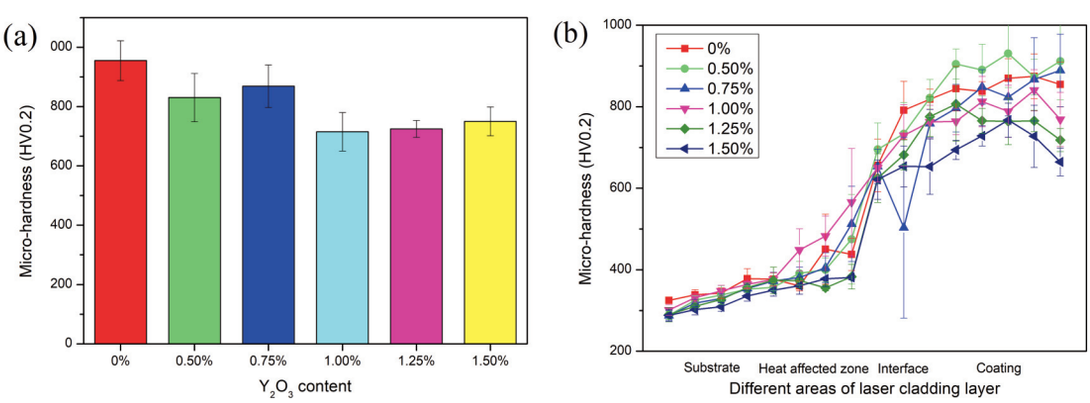

Figure 6. *The surface micro-micro-hardness of in-situ synthesized WC reinforced nickel base cladding layer with different content of Y_2O_3: (a) the surface micro-micro-hardness, (b) the cross-section micro-micro-hardness*

values of the cladding layers showed large fluctuations at the interface, probably due to dissolution in the WC hard phase organization at the bottom layer of these cladding layers, resulting in much less micro-hardness in this area than at other parts.

Overall, the micro-hardness distribution of both fused cladding layers doped with different contents of Y_2O_3 or CeO_2 is uniform, and all cladding layers have a micro-hardness transition zone between the coating and the substrate. The doping of both rare-earth oxides caused a slight decrease in the micro-hardness of the fused cladding layers, but the micro-hardness of all fused cladding layers was still much higher than that of the substrate. In addition, the maximum micro-hardness of the fused clad layers doped with different contents of Y_2O_3 was slightly higher than that of the fused clad layers doped with different contents of CeO_2.

3.2.2. Reciprocating friction wear performance

Figures 7 and 8 show the average friction coefficient and the wear amount, the friction coefficient curve and the wear scar morphology of the in situ grown WC-reinforced nickel-based fused cladding layers doped with different contents of CeO_2 for dry grinding and wet grinding under emulsion environment, respectively. With the gradual increase of the doped CeO_2 content, the dry friction wear resistance of the molten cladding layer first appeared to be enhanced and then decreased. When the CeO_2 content reached 0.75%, the strengthening effect of CeO_2 on the wear resistance of the molten cladding layer reached the maximum, and the average friction coefficient of the molten cladding layer was 0.194 at this time, and the friction coefficient curve was a straight line with less fluctuation, which indicated that the hard particles in the molten cladding layer had a better refining effect. At this time, the average friction coefficient of the cladding layer was 0.194, and the friction coefficient curve was straight line with less fluctuation, which means that the hard particles in the cladding layer were better refined at this time, and they shed less during the frictional wear process. The wear scar morphologies in Fig. 8(a) show obvious spalling pit morphology, which indicates that a large amount of WC hard phase particles is shed during the frictional wear process, at which time the wear mechanism of the fused layer is abrasive wear and adhesive wear.

Wet grinding in emulsion environment, the wear resistance of each molten layer had a smaller friction coefficient and wear amount, while the wet grinding wear resistance of the molten layer doped with different contents of CeO_2 had a significant strengthening effect compared with that of the cladding layer not doped with CeO_2, which is related to the grain refining effect of CeO_2 on the laser molten layer. The friction coefficient curves of the CeO_2-doped cladding layer are relatively gentle straight lines, indicating that the cladding layer did not have obvious hard phase shedding during the wet grinding friction wear process, and the surface of the cladding layer did not cause serious damage. The wear resistance of the molten cladding layer increased and then decreased as the CeO_2 content gradually increased, and when the CeO_2 content was 0.75%, the wear resistance of the molten cladding layer in wet grinding was the best, and the average friction coefficient in wet grinding was 0.032. The wear scar morphology in Fig. 8(b) shows that there is no obvious damage to the surface of the molten cladding layer in wet grinding under the emulsion environment, and only slight scratches exist. The rare-earth elements can make the molten cladding layer grain refinement, uniform composition distribution and dense organization, and produce some rare-earth reinforced phases, thus improving the wear resistance of the molten cladding layer. In addition, the addition of rare earth elements can effectively strengthen the wear resistance of the molten cladding layer when the

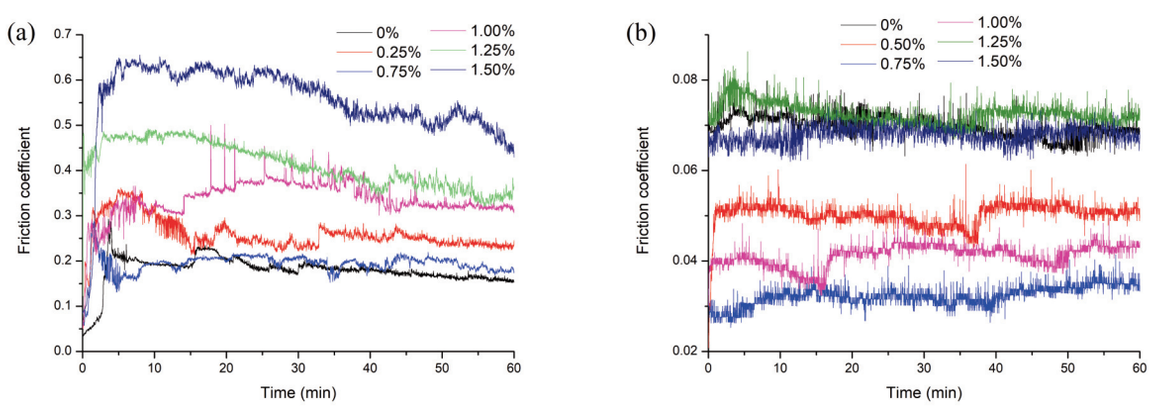

Figure 7. *The friction coefficient curve of in-situ synthesized WC reinforced nickel base cladding layer with different content of CeO_2: (a) dry grinding, (b) wet grinding*

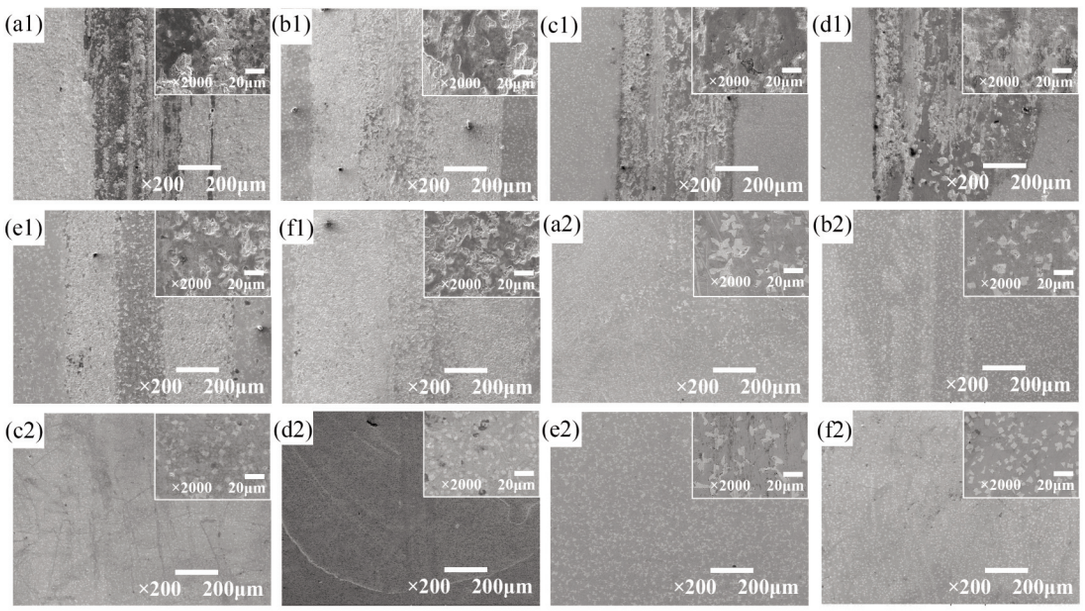

Figure 8. *The wear scar morphologies of in-situ synthesized WC reinforced nickel base cladding layer with different content of CeO_2: (a) 0%, (b) 0.50%, (c) 0.75%, (d) 1.00%, (e) 1.25%, (f) 1.50%; (1) dry grinding, (2) wet*

content of rare earth elements reaches a certain level, but when the content of rare earth elements exceeds a certain level, the strengthening effect on the wear resistance of the molten cladding layer decreases.

The average friction coefficients and wear amounts, friction coefficient graphs and wear scar morphologies of the enhanced nickel-based fused cladding layers doped with different contents of Y_2O_3 for dry grinding and wet grinding under emulsion environment are shown in Figures 9 and 10. The analysis shows that there was no obvious linear relationship between the dry grinding wear resistance of the fused layers and the content of doped Y_2O_3 during dry friction wear. When the Y_2O_3 content was 0.75% and 1.50%, the wear resistance of the molten cladding layer was the best, and the average friction coefficients were 0.261 and 0.296 respectively at this time, and the friction coefficient graph was flatter at this time, and the in situ grown WC particle enhancement phase was refined, and the small particles were not easily dislodged, which strengthened the wear resistance of the molten cladding layer. In Fig. 10(a), there is not much difference in the width of the wear marks of each cladding layer, and the wear marks of the cladding layer doped with rare earth oxide Y_2O_3 are lighter than those of the cladding layer not doped with Y_2O_3, which also indicates that Y_2O_3 has a positive effect on the wear resistance of the cladding layer. Currently, the dry friction wear mechanism of the molten cladding layer was obvious adhesion wear and abrasive wear.

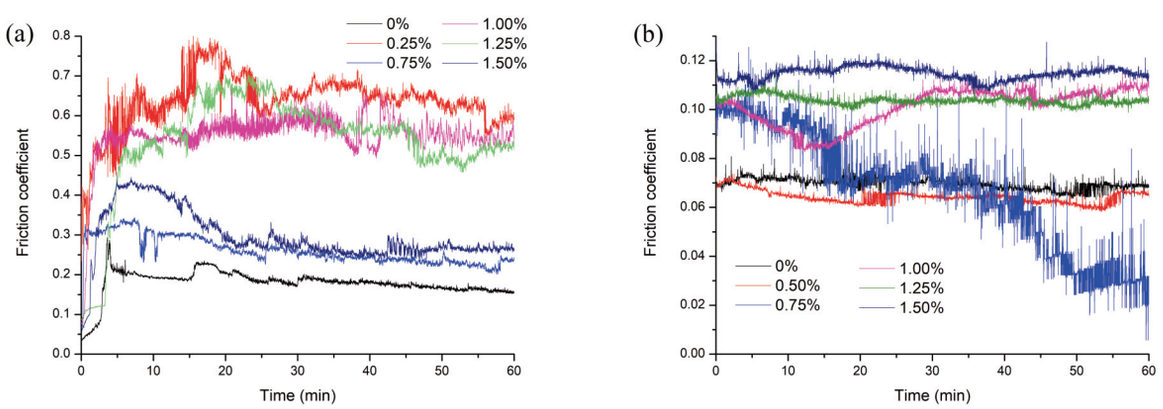

Figure 9. *The friction coefficient curve of in-situ synthesized WC reinforced nickel base cladding layer different content of Y_2O_3: (a) dry grinding, (b) wet grinding*

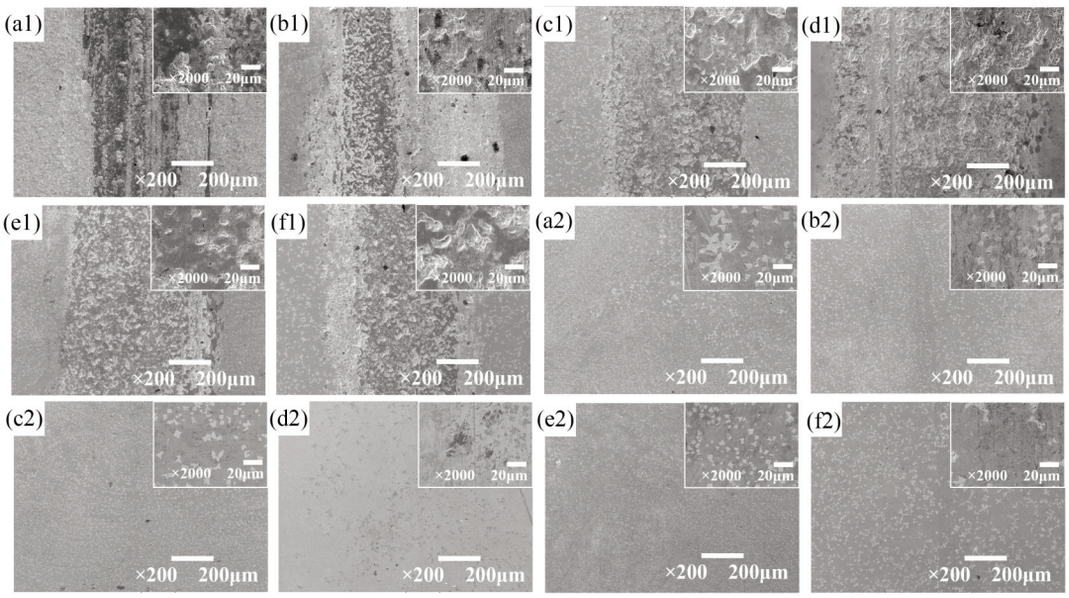

Figure 10. *The wear scar morphologies of in-situ synthesized WC reinforced nickel base cladding layer with different content of Y_2O_3: (a) 0%, (b) 0.50%, (c) 0.75%, (d) 1.00%, (e) 1.25%, (f) 1.50%; (1) dry grinding, (2) wet*

In the wet grinding under emulsion environment, when the Y_2O_3 content was 0.50%, the wet grinding wear resistance of the molten layer was the best. Currently, the average friction coefficient of the molten layer was 0.064 and the wear amount was 1.0 mg, and the friction coefficient curve was smooth without large fluctuations, which indicates that the wear resistance of the molten layer was good and there is no destructive damage. When the Y_2O_3 content was 0.75%, the average friction coefficient of the molten layer was slightly larger than that of the molten layer with the content of 0.50%, which was 0.067, but the friction coefficient curve graph at this time was more fluctuating, which indicates that a small amount of hard phase particles was shed from the surface of the molten layer during the frictional wear process leading to the occurrence of secondary wear. In Figure 10(b), in the emulsion environment, the emulsion had a better lubrication and protection effect on the molten layer, and the wear marks on the surface of the molten layer were lighter, and the molten layer did not produce larger damage within 60 min of the experiment.

4. Effect of rare earth doped on the electrochemical properties of the molten cladding layer

Figure 11 shows the electrochemical polarization graphs, impedance plots and bode plots of the in situ grown WC-reinforced nickel-based melt cladding layers doped with different contents of CeO_2. When the CeO_2 content was 0.50%, 0.75% and 1.50%, the corrosion resistance of the molten cladding layer was stronger than that of the molten cladding layer doped with CeO_2, but the relationship between the corrosion resistance of the molten cladding layer and the CeO_2 content was not obvious. The corrosion resistance of the melt layer was best when the CeO_2 content was 1.50%, and the self-corrosion potential and self-corrosion current density of the melt layer were -0.12549 V and 2.355×10^{-7} A/cm_2, respectively, and the coating resistance and charge transfer resistance Rct1 were 395600 and 5823 Ω·cm_2, respectively, and the coating capacitance and double-layer interface capacitance were 1.5425×10^{-5} and 2.1221×10^{-5} $Ω^{-1}$ Sncm^2, respectively.

At this time, the appropriate amount of rare earth oxide CeO_2 had a positive effect on the corrosion resistance of the melt cladding layer, and the optimal CeO_2 content in the in situ grown WC hard particle reinforced nickel-based melt cladding layer was 1.50%. When the CeO_2 content was 0%, 0.50% and 1.50%, an obvious passivation phenomenon appeared in the polarization curve of the molten cladding layer, and a passivation film was generated on the surface of the molten cladding layer during the electrochemical test, which hindered the contact between the corrosive medium and the molten cladding layer and slowed down the dissolution of the corrosive medium into the particle phase, and had a positive effect on the corrosion resistance of the molten cladding layer.

Fig. 12 shows the electrochemical polarization curves, impedance and bode plots of the in situ grown WC-reinforced nickel-based fused cladding layers doped with different contents of Y_2O_3. The self-corrosion current densities were 5.1123×10^{-6} and 1.9170×10^{-7} A/cm^2 when the Y_2O_3 content was 0.75%

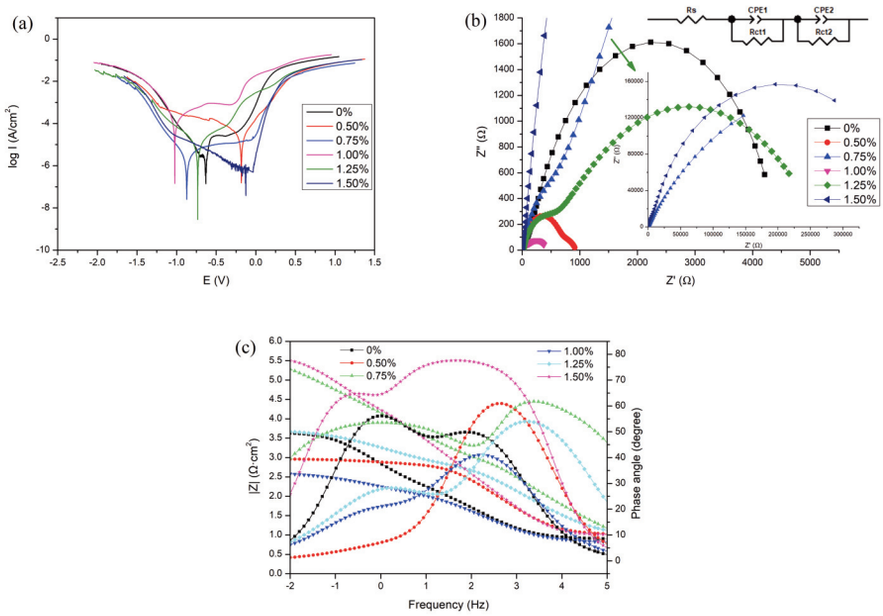

Figure 11. *The electrochemical properties of in-situ synthesized WC reinforced nickel base cladding layer with differen content of CeO_2: (a) polarization curve, (b) impedance diagram, (c) bode diagram*

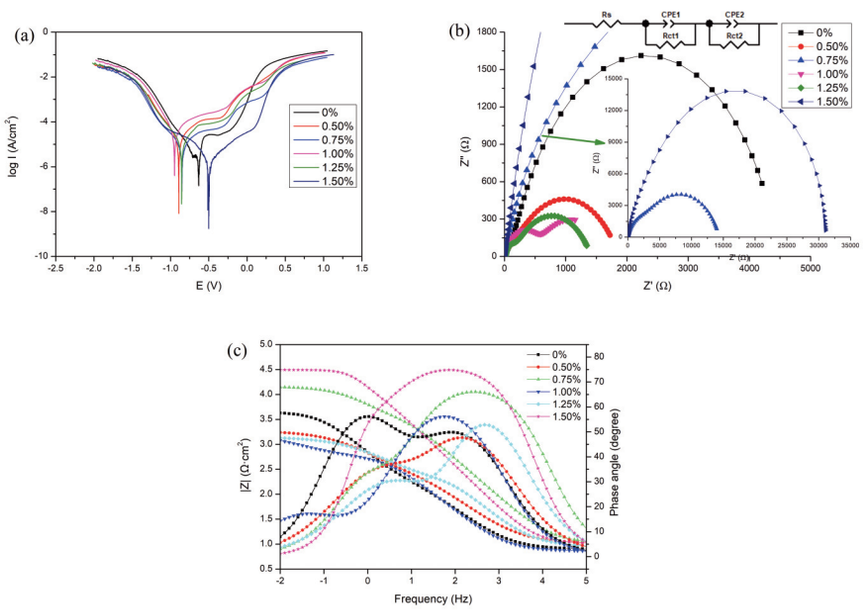

Figure 12. *The electrochemical properties of in-situ grown WC reinforced nickel base cladding layer with different content of Y_2O_3: (a) polarization curve, (b) impedance diagram, (c) bode diagram*

and 1.50%, respectively, which were smaller than those of the undoped Y_2O_3 melt cladding layer, i.e., 6.7675×10^{-6} A/cm^2, while the self-corrosion current densities of the other melt cladding layers were much larger than that of the undoped Y_2O_3 melt cladding layer.

Meanwhile, it can be found in the impedance diagram that only when the Y_2O_3 content was 0.75% and 1.50%, the corrosion resistance of the molten cladding layer was stronger than that of the molten cladding layer without Y_2O_3 doping, which showed that only the appropriate amount of Y_2O_3 doping also had a strengthening effect on the corrosion resistance of the molten cladding layer, and with the increase of Y_2O_3 content, the corrosion resistance of the molten cladding layer first decreased and then appeared to increase.

The best corrosion resistance of the melt layer was

achieved when the Y_2O_3 content was 1.50%, at which the self-corrosion potential and corrosion potential of the melt layer were -0.49924 V and 1.9170×10^{-7} A/cm^2, respectively, and the coating resistance and charge transfer resistance were 5476 and 25631 Ω·cm^2, respectively, and the coating capacitance and double-layer interface capacitance were 2.0383×10^{-5} and 1.3874×10^{-5} Ω^{-1}Sncm^2, respectively.

5. Conclusions

In this work, the in situ grown WC-reinforced nickel-based melt cladding layer was prepared, and the effects of doping with different contents of rare earth oxides on the microstructure and properties of the cladding layer was investigated, and the effects of doping with different contents of rare earth oxides CeO_2 and Y_2O_3 on the micro-hardness, microstructure, wear resistance and corrosion resistance of the cladding layer were investigated. The obtained results are as follows.

The reinforcing phase was uniformly distributed throughout the coating and there were no holes or cracks in the in-situ synthesized coating. As the content of CeO_2 and Y_2O_3 increased, the original WC particles in the cladding layer gradually increased in size, and the WC bulk particles in the cladding layer were most uniformly distributed when the doped CeO_2 content was 0.75 and the Y_2O_3 content was 1.5, which had a positive effect on the enhancement of the wear and corrosion resistance of the cladding layer.

The maximum micro-hardness of the fused cladding layers doped with different contents of CeO_2 and Y_2O_3 was 860 HV0.2 and 870 HV0.2, which was slightly lower than that of the undoped fused cladding layer when the CeO_2 content was 1% and the Y_2O_3 content was 0.75%, respectively.

There is no obvious linear relationship between the friction resistance of the cladding layer and the content of CeO_2 and Y_2O_3 doping, and the best wear resistance of the cladding layer was achieved when the CeO_2 content was 1% and the Y_2O_3 content was 0.75%. The wear mechanism of the cladding layer was still dominated by abrasive and adhesive wear.

The appropriate amount of rare earth oxides had a positive effect on the wear and corrosion resistance of the cladding layer, and when the content of rare earth oxides was too high, the performance of the cladding layer was decreased. When the CeO_2 content was 1.50% and the Y_2O_3 content reached 1.50%, the corrosion resistance of the cladding layer was the excellent.

Funding

The work was supported by the key research and development project of Shaanxi Province [Grant No. 2021SF-469] and the National Natural Science Foundation of China [Grant No.52175184].

Conflicts of interest

The authors declare no financial or commercial conflict of interest.

Availability of data and material

The datasets generated during and analyzed during the current study are available from the corresponding author on reasonable request.

Authors' contributions

Cong-xiao Zhang and Wan-chang Sun conceived the idea of the study, analyzed most of the data and wrote the initial draft of the paper; Er-yong Liu and Yu-wan Liu analyzed the data; the remaining authors contributed to refining the ideas, carrying out additional analyses and finalizing this paper. All authors discussed the results and revised the manuscript.

References

[1] L. Huang, J.Z. Zhou, J. Xu, Microstructure and wear resistance of electromagnetic field assisted multi-layer laser clad Fe901 coating, Surface & Coatings Technology, 395 (2020) 125876. https://doi.org/10.1016/j.surfcoat.2020.125876.

[2] B.C. Li, H.M. Zhu, C.J. Qiu, Development of high strength and ductile martensitic stainless steel coatings with Nb addition fabricated by laser cladding, Journal of Alloys & Compounds, 832 (2020). https://doi.org/10.1016/j.jallcom.2020.154985.

[3] L.L. Zhai, C.Y. Ban, J.W. Zhang, Investigation on laser cladding Ni-base coating assisted by electromagnetic field, Optics and Laser Technology, 114 (2019) 81-88. https://doi.org/10.1016/j.optlastec.2019.01.017.

[4] R. Zhu, C.Y. Zhu, S. Wu, Effect of CeO_2 on Microstructure and properties of Ni-Co-based coatings, Journal of Materials Research and Technology, 26 (2023) 7329-7339. https://doi.org/10.1016/j.jmrt.2023.09.108.

[5] X. Kang, L.Y. Chen, L.J. Chai, Microstructural characteristics and properties of CoCrFeNiNbx high-entropy alloy coatings on pure titanium substrate by pulsed laser cladding. Applied Surface Science, 517 (2020) 146214. https://doi.org/10.1016/j.apsusc.2020.146214.

[6] Y. Liu, Y. Wu, Y. Ma, High temperature wear performance of laser cladding Co06 coating on high-speed train brake disc, Applied Surface Science, 481 (2019) 761-766. https://doi.org/10.1016/j.apsusc.2019.02.235.

[7] M. Li, B. Han, L. Song, Enhanced surface layers by laser cladding and ion sulfurization processing towards improved wear-resistance and self-lubrication performances, Applied Surface Science, 503 (2020) 144226.1-144226.11.

https://doi.org/10.1016/j.apsusc.2019.144226.

[8] T. Rong, D. Gu, Q. Shi, Effects of tailored gradient interface on wear properties of WC/Inconel 718 composites using selective laser melting, Surface & Coatings Technology, 307 (2016) 418-27. https://doi.org/10.1016/j.surfcoat.2016.09.011.

[9] Y. Li, C. Hou, H. Lu, WC strengthened W-Cu nanocomposite powder synthesized by in-situ reactions, International Journal of Refractory Metals & Hard Materials, 79 (2019) 154-157. https://doi.org/10.1016/j.ijrmhm.2018.12.003.

[10] G. Muvvala, D.P. Karmakar, A.K. Nath, In-process detection of microstructural changes in laser cladding of in-situ Inconel 718/TiC metal matrix composite coating, Journal of Alloys & Compounds, 740 (2018) 545-558. https://doi.org/10.1016/j.jallcom.2017.12.364.

[11] M. Zhong, W. Liu, Laser surface cladding: The state of the art and challenges, Proceedings of the Institution of Mechanical Engineers part C-The Journal of Mechanical Engineering Science, 224(5) (2010) 1041-1060. https://doi.org/10.1243/09544062JMES1782.

[12] B.S. Yilbas, S.S. Akhtar, C. Karatas, Laser surface treatment of Inconel 718 alloy: thermal stress analysis, optics and lasers in engineering, 48(7-8) (2010) 740-749. https://doi.org/c 10.1016/j.optlaseng.2010.03.012.

[13] H. Zhu, Y. Li, B. Li, Z. Zhang, C. Qiu, Effects of low-temperature tempering on microstructure and properties of the laser-cladded AISI 420 martensitic stainless steel coating, Coatings, 8(12) (2018) 451. https://doi.org/10.3390/coatings8120451.

[14] F. Hao, B. Liao, D. Li, Effects of rare earth oxide on hardfacing metal microstructure of medium carbon steel and its refinement mechanism, Journal of Rare Earths, 029(006) (2011) 609-613. https://doi.org/10.1016/s1002-0721(10)60507-8

[15] C. Zhang, H. Hu, L. Mao, Effect of Y_2O_3 content on the microstructure and wear performance of plasma-sprayed Cr_2O_3–Y_2O_3 composite coatings, Ceramics International, 50(3) (2024) 4553-4562. https://doi.org/10.1016/j.ceramint.2023.11.194.

[16] T.G. Zhang, H.F. Zhuang, Q. Zhang, Influence of Y_2O_3 on the microstructure and tribological properties of Ti-based wear-resistant laser-clad layers on TC4 alloy, Ceramics International, 46(9) (2020) 13711-13723. https://doi.org/10.1016/j.ceramint.2020.02.159.

[17] L. He, Z. Xu, X. Cao, Adhesive strength of new thermal barrier coatings of rare earth zirconates, Vacuum, 83(11) (2009) 1388-1392. https://doi.org/10.1016/j.vacuum.2009.04.053.

[18] Z.Q. Zhang, Q. Yang, Z. M. Yu, Influence of Y_2O_3 addition on the microstructure of TiC reinforced Ti-based composite coating prepared by laser cladding, Materials Characterization, 189 (2022) 111962. https://doi.org/10.1016/j.matchar.2022.111962.

[19] C.F. Wu, M.X. Ma, W. Liu, Laser cladding in-situ carbide particle reinforced Fe-based composite coatings with rare earth oxide addition, Journal of Rare Earths, 27(6) (2009) 997-1002. https://doi.org/10.1016/S1002-0721(08)60377-4.

[20] X. Xing, Z. Han, H. Wang, Electrochemical corrosion resistance of CeO_2-Cr/Ti i coatings on 304 stainless steel via pack cementation, Journal of Rare Earths, 33(10) (2015) 1122-1128. https://doi.org/10.1016/S1002-0721(14)60535-4.

[21] K.L. Wang, Q.B. Zhang, M.L. Sun, Rare earth elements modification of laser-clad nickel-based alloy coatings, Applied Surface Science, 174(3-4) (2001) 191-200. https://doi.org/10.1016/S0169-4332(01)00017-4.

[22] D.Q. Yu, J. Zhao, L. Wang, Improvement on the microstructure stability, mechanical and wetting properties of Sn–Ag–Cu lead-free solder with the addition of rare earth elements, Journal of Alloys & Compounds, 376(1-2) (2004) 170-175. https://doi.org/10.1016/j.jallcom.2004.01.012.

[23] J. Li, X. Luo, G.J. Li, Effect of Y_2O_3 on the sliding wear resistance of TiB/TiC-reinforced composite coatings fabricated by laser cladding, Wear, 310(1-2) (2014) 72-82. https://doi.org/10.1016/j.wear.2013.12.019.

[24] D.S. Wang, E.J. Liang, M.J. Chao, Investigation on the microstructure and cracking susceptibility of laser-clad V2O5 /NiCrBSiC alloy coatings, Surface & Coatings Technology, 202(8) (2008) 1371-1378. https://doi.org/10.1016/j.surfcoat.2007.06.036.

[25] R. Zhu, Z. Li, X. Li, Microstructure and properties of the low-power-laser clad coatings on magnesium alloy with different amount of rare earth addition, Applied Surface Science, 353 (2015) 405-413. https://doi.org/10.1016/j.apsusc.2015.06.071.

[26] S.C. Tjong, Z.Y. Ma, Microstructural and mechanical characteristics of in situ metal matrix composites, Materials Science and Engineering R: Reports, 29(3) (2000) 49-113. https://doi.org/10.1016/s0927-796x(00)00024-3.

[27] C. Yang, C.N. Jing, T.L. Fu, Effect of CeO_2 on the microstructure and properties of $AlCoCrFeNi_{2.1}$ laser cladding coatings, Journal of Alloys and Compounds, 976 (2024) 172948. https://doi.org/10.1016/j.jallcom.2023.172948.

[28] J. Prywer, Explanation of some peculiarities of crystal morphology deduced from the BFDH law, Journal of crystal growth, 270(3-4) (2004) 699-710. https://doi.org/10.1016/j.jcrysgro.2004.06.046.

[29] X.F. Wan, C. Tian, Y. Li, Effect of Y_2O_3 addition on microstructure and properties of laser cladded Al-Si coatings on AZ91D magnesium alloy, Materials, 16(1) (2023) 338. https://doi.org/10.3390/ma16010338.

[30] L. Xu, X.L. Yin, N. Wang, Effect of Y_2O_3 addition on the densification, microstructure and mechanical properties of $MgAl_2O_4CaAl_4O_7CaAl_{12}O_{19}$ composites, Journal of Alloys and Compounds, 702 (2017) 472-478. https://doi.org/10.1016/j.jallcom.2017.01.282.

EFEKTI CeO_2/Y_2O_3 OKSIDA RETKE ZEMLJE NA MIKROSTRUKTURU I OSOBINE IN-SITU SINTETISANOG SLOJA OBLOGE OJAČANOG WC-OM NA BAZI NIKLA

C.-X. Zhang, W.-C. Sun*, E.-Y. Liu, Y.-W. Liu, J.-P. Liu, B. Zhang, Y.-F. Xu, M.-R. Zhou**

Fakultet za nauku o materijalima i inženjerstvo, Univerzitet za nauku i tehnologiju u Sijanu, Sijan, Šansi, Kina

Apstrakt

Inovativni sloj laserske obloge na bazi nikla (Ni) ojačan volfram-karbidom (WC) pripremljen je kroz proces in-situ sinteze. Analiziran je uticaj različitih koncentracija CeO_2/Y_2O_3 na mikrostrukture, otpornost na habanje i otpornost na koroziju in-situ sintetisanog sloja obloge ojačanog WC-om na bazi nikla. Rezultati su pokazali da prevlake dopirane oksidima retkih zemalja pokazuju dobru mikrotvrdoću (660 HV0.2) i otpornost na habanje kada sadržaj oksida retkih zemalja dostigne 0,75% CeO_2 i 1,50% Y_2O_3. Pored toga, minimalne brzine korozije prevlaka izmerene su na 0,002770 mm/god i 0,0022548 mm/god pri dopingu od 1,5% CeO_2 i 1,5% Y_2O_3, sa E_{corr} vrednostima u rasponu od -0,12549 V do -0,49924 V i nižim I_{corr} vrednostima u rasponu od $2,3550\times10^{-7}$ A•cm^2 do $1,9170\times10^{-7}$ A•cm^2. Nadalje, otpornost na habanje sloja obloge bila je značajno viša od otpornosti podloge. I sloj obloge i podloga su pokazali mešoviti način habanja, i pokazuju adheziono habanje u uslovima mokrog trenja.

Ključne reči: *Laserska obloga; In-situ sinteza; Retke zemlje; Mehaničke osobine; Elektrohemijske osobine*